

**EXPERIMENTAL AND SIMULATION STUDIES ON THE EFFECT OF
CYLINDER SIZE ON AERODYNAMIC DRAG COEFFICIENT**

KUAT TELEGENOV

UNIVERSITI TEKNOLOGI MALAYSIA

DECLARATION OF THESIS / UNDERGRADUATE PROJECT PAPER AND COPYRIGHT

Author's full name : **KUAT TELEGENOV**

Date of birth : **02 FEBRUARY 1988**

Title : **EXPERIMENTAL AND SIMULATION STUDIES ON THE EFFECT**

OF CYLINDER SIZE ON AERODYNAMIC DRAG COEFFICIENT

Academic Session: **2011-2012**

I declare that this thesis is classified as:

CONFIDENTIAL

(Contains confidential information under the Official Secret Act 1972)*

RESTRICTED

(Contains restricted information as specified by the organization where research was done)*

OPEN ACCESS

I agree that my thesis to be published as online open access (full text)

I acknowledged that Universiti Teknologi Malaysia reserves the right as follows:

1. The thesis is the property of Universiti Teknologi Malaysia.
2. The Library of Universiti Teknologi Malaysia has the right to make copies for the purpose of research only.
3. The Library has the right to make copies of the thesis for academic exchange.

Certified by:

SIGNATURE

200707M10030
(NEW IC NO. /PASSPORT NO.)

SIGNATURE OF SUPERVISOR

ISKANDAR SHAH BIN ISHAK
NAME OF SUPERVISOR

Date: _____

Date: _____

NOTES : * If the thesis is CONFIDENTIAL or RESTRICTED, please attach with the letter from the organization with period and reasons for confidentiality or restriction.

“I hereby declare that I have read this thesis and in my opinion this thesis is sufficient in terms of scope and quality for the award of the degree of Bachelor of Engineering (Aeronautics)”

Signature : _____

Name of Supervisor : Iskandar Shah bin Ishak

Date : _____

EXPERIMENTAL AND SIMULATION STUDIES ON THE EFFECT OF
CYLINDER SIZE ON AERODYNAMIC DRAG COEFFICIENT

KUAT TELEGENOV

A report submitted in fulfillment of the
requirements for the award of the degree of
Bachelor of Mechanical Engineering (Aeronautics)

Faculty of Mechanical Engineering
Universiti Teknologi Malaysia

JANUARY 2012

I declare that this thesis entitled “Experimental and simulation studies on the effect of cylinder size on aerodynamic drag coefficient” is the result of my own research except as cited in the references.

Signature : _____

Name : Kuat Telegenov

Date : _____

To my beloved mother and father

ACKNOWLEDGEMENT

First and above all, I am very grateful to Allah, with His blessing, allow me to complete this project in time.

I would like to take this opportunity to express my deep sense of gratitude and appreciation to my project advisor, Professor Iskandar Shah bin Ishak. His endless help, useful information, support, advice and guidance have made it possible for me to finish the project successfully.

Special thanks to all personnel of Faculty of Mechanical Engineering, UTM. Especially, thanks to staff in UTM wind tunnel facility, their help was very important in conducting experiment.

Thanks to all those who have made a contribution to my project

ABSTRACT

The purpose of this study is to investigate the effect of circular cylinder size on aerodynamics drag coefficient by conducting wind tunnel test and simulation approach. These investigations were conducted at four different size of cylinders at various test wind speed. The experimental results from the conducted wind tunnel test were compared with established data. The results are found to be agreeable with each other. In addition simulation results are also in parallel with the experimental results, thus verifying the methodology opted for the simulation works.

ABSTRAK

Objektif kajian ini adalah untuk menyelidik kesan saiz silinder ke atas pekali daya seret dengan mengadakan pengujian terowong angin dan simulasi berkomputer. Penyelidikan ini dilakukan ke atas empat silinder yang berlainan saiz pada beberapa kelajuan angin tertentu. Perbandingan keputusan ujikaji telah dibuat dengan kertas kerja rujukan dan didapati keputusannya adalah sejajar. Di samping itu, keputusan simulasi komputer juga didapati selari dengan keputusan ujikaji, dan ini mensahkan kaedah simulasi yang telah digunakan dalam projek ini.

TABLE OF CONTENTS

CHAPTER	TITLE	PAGE
	DECLARATION	ii
	DEDICATION	iii
	ACKNOWLEDGEMENTS	iv
	ABSTRACT	v
	ABSTRAK	vi
	TABLE OF CONTENTS	vii
	LIST OF TABLES	x
	LIST OF FIGURES	xii
	LIST OF ABBREVIATIONS	xiii
	LIST OF SYMBOLS	xiv
	LIST OF APPENDICES	xvi
1	INTRODUCTION	1
1.1	Project background	1
1.2	Project scope	1
1.3	Project objective	2
1.4	Significance of study	2
2	LITERATURE REVIEW	3
2.1	Introduction	3
2.2	General flow theory	3
2.3	Flow field around a circular cylinder	7
2.4	Drag coefficient of a circular cylinder	8

2.5	Transitions around a circular cylinder	12
2.6	Surface roughness effects	13
2.7	Finite cylinder	13
2.8	Boundary corrections of wind tunnel data	14
2.9	Computational fluid dynamics	16
2.9.1	Equations describing flow	16
2.9.2	Navier-Stokes equations	17
2.9.3	Turbulence models	18
2.9.3.1	The k-e turbulence model	18
2.9.3.2	Realizable k-e model	19
2.9.4	Mesh statistics	19
2.9.4.1	Skewness	19
2.9.4.2	Aspect ratio	20
3	APPARATUS AND SOFTWARE	22
3.1	Wind tunnel	22
3.1.1	Introduction	22
3.1.2	UTM Wind Tunnel	25
3.2	Drag measurement	27
3.3	Software	28
3.3.1	Introduction to ANSYS	28
3.3.2	Computational fluid dynamics	28
4	METHODOLOGY	30
4.1	Introduction	30
4.2	Experimental setup	30
4.3	Wind tunnel testing	32
4.4	Testing models	33
4.5	Computational fluid dynamics (CFD)	34
4.5.1	Geometry	35
4.5.2	Meshing	36
4.5.3	Boundary conditions	37
4.5.4	Turbulence model	37
4.5.5	Fluent analysis	37

4.5.6	Post-processing	38
5	RESULTS AND DISCUSSION	39
5.1	Introduction	39
5.2	Experimental results	39
5.3	Verification of the results	43
5.4	Grid independence analysis	45
5.5	Mesh statistics results	46
5.6	Discussion	47
6	CONCLUSION	48
REFERENCES		49
Appendices A-C		51-52

LIST OF TABLES

TABLE NO.	TITLE	PAGE
2.1	Flow regime at a circular cylinder (Schlichting, 1979)	11
2.2	Drag coefficients for finite-length circular cylinder with free ends	14
3.1	Balance load range	27
4.1	Reynolds number at different speed with different diameter	31
5.1	Results from experiment	40

LIST OF FIGURES

FIGURE NO.	TITLE	PAGE
2.1	Superposition of a uniform flow and a doublet; nonlifting flow over a circular cylinder (Anderson, 2007)	4
2.2	Hydrogen bubble visualization of the separated water flow around a cylinder at a Reynolds number of 0.2×10^6 (Courtesy of K.W.McAlister and L.W.Carr, U.S. Army Aeroflightdynamics Directorate, AVSCOM)	6
2.3	Theoretical pressure distribution (solid curve) around a cylinder compared with experimental data at Reynolds number of 6.7×10^5 (chain curve) (Schlichting, 1979)	7
2.4	Flow field around circular cylinder	8
2.5	Typical experimental results for the drag coefficient for cylinders and spheres as function of Reynolds number(Schlichting, 1979)	9
2.6	C_D vs. Re for infinite cylinder (Tritton,1988)	9
2.7	Circular cylinder: drag coefficient vs. Reynolds number	10
2.8	Variation of C_D and Flow Transitions for circular cylinder flow (Zdravkovich, 1997)	12
2.9	Effects of roughness parameter on drag coefficient (Zdravkovich)	13
2.10	Values of τ_1 for a number of tunnel types (Barlow)	16
2.11	Skewness in meshing	20
2.12	Aspect ratio in meshing	21

3.1	Plan view of an open circuit wind tunnel (Diamler-Benz Aerospace Airbus, Bremen, Germany)	23
3.2	A closed circuit wind tunnel, Defense Establishment Research Agency (DERA), 13x9-ft tunnel in Bedford, England	24
3.3	Plan of UTM Low-Speed Wind Tunnel Facility	25
3.4	Transfer of aerodynamics forces and moments to the balance load cell	27
4.1	Placement of cylinder in the test section	32
4.2	Flowchart for experiment	33
4.3	Flowchart for CFD simulation	35
4.4	Geometry	36
5.1	Drag force versus wind speed	41
5.2	Drag coefficient versus wind speed	41
5.3	Drag force versus diameter	42
5.4	Drag coefficient versus diameter	42
5.5	Drag coefficient versus Reynolds number(32mm)	43
5.6	Drag coefficient versus Reynolds number(50mm)	44
5.7	Drag coefficient versus Reynolds number(65mm)	44
5.8	Drag coefficient versus Reynolds number(75mm)	45
5.9	Drag force versus number of elements at 10m/s (32mm)	46
5.10	Mesh statistics from simulation	46

LIST OF ABBREVIATIONS

AC	-	Alternating current
AVSCOM	-	Army Aviation Systems Command
CFD	-	Computational Fluid Dynamics
DERA	-	Defense Establishment Research Agency
LST	-	Low Speed Tunnel
NPL	-	National Physical Laboratory
RANS	-	Reynolds-Averaged Navier-Stokes
RNG	-	Re-Normalisation Group
SST	-	Shear Stress Transport
UTM	-	Universiti Teknologi Malaysia

LIST OF SYMBOLS

b	-	Model geometric span
B	-	Tunnel breadth
C_D	-	Drag coefficient
C_{df}	-	Friction drag coefficient
C_{dp}	-	Pressure drag coefficient
C_p	-	Pressure coefficient
d, D	-	Diameter
F_D, F	-	Drag force
h	-	Height
k	-	Doublt strength
K_s/d	-	Roughness parameter
L	-	Length
p	-	Pressure
r	-	Radius
Re	-	Reynolds number
u	-	Velocity in the stream wise direction
V	-	Velocity
V_r	-	Radial velocity
V_u	-	Uncorrected velocity
V_θ	-	Tangential velocity
V_∞	-	Free stream velocity
x, y	-	Displacement
ε	-	Solid blockage factor
θ	-	Angle
μ	-	Dynamic viscosity

ν	-	Kinematic viscosity
π	-	Pi constant (3.14159)
ρ	-	Density
τ_1	-	Factor depending on the tunnel test-section shape and the model span-to-tunnel width ratio
Ψ	-	Stream function

LIST OF APENDICES

APPENDIX	TITLE	PAGE
A	Meshing of the domain	51
B	Inflation	52
C	Sectioning of meshed cylinder	53

CHAPTER 1

INTRODUCTION

1.1 Project Background

Aerodynamic drag is the fluid drag force that acts on any moving solid body in the direction of the fluid free stream flow. There are a few factors that affect the drag force that an object experiences. These factors are shape, fluid medium, speed and the object's surface. Engineers can manipulate these factors in order to minimize or maximize the drag. In most cases drag forces need to be known to design other parameters such as engine power to overcome drag, structural strength and materials to be used. In this project to investigate the drag coefficient's characteristics of a circular cylinder, wind tunnel test and CFD simulation of different shaped cylinders at various free stream speeds will be conducted.

1.2 Project scope

- a) Literature review on aerodynamic drag coefficient of a circular cylinder.

- b) Build wind tunnel models of a cylinder.
- c) Conduct the wind tunnel test and CFD simulation on different sizes of cylinder to determine the aerodynamic drag coefficient and its characteristics at various test wind speed.
- d) Compare the wind tunnel and CFD simulation results and analyze them.

1.3 Project objective

To investigate the effect of cylinder size on aerodynamics drag coefficient by conducting the wind tunnel test and simulation work.

1.4 Significance of study

In theory and general understanding, the different sizes of cylinder must have the same coefficient of drag, since the same aerodynamic shape should have same aerodynamics characteristics. Therefore this project aims to quantify the statement by doing the numerical and experimental studies. The significance of this study is to investigate the effect of different sizes of cylinder on drag coefficient. In addition effect of wind speed on aerodynamic drag will be also analyzed. It could help in designing and building vehicles, buildings and other civil structures that are using cylinders as component. It's very important to know for engineers when they choosing the cylinder as the main structural part to know the effect of cylinder's size and its speed on drag coefficient. Apart of that, the project will determine either the subcritical speed, where the drag coefficient starts become constant with the wind speed, is independent of cylinder's size.

CHAPTER 2

LITERATURE REVIEW

2.1 Introduction

Generally study on flow around a circular cylinder is popular field. Many studies have been done before (Zdravkovich, 1997; Roshko, 1961; Finn, 1953), they had different objectives, scopes and different parameters were obtained. Those parameters are lift and drag coefficients, pressure distribution, effects of turbulence, etc. The experiments were conducted by wind tunnel either CFD simulation, but sometimes two mentioned testing procedures were used together to compare the results.

2.2 General flow theory

Consider a uniform flow with free stream velocity, V_∞ and a doublet of strength, k as shown in Figure 2.1. The direction of the doublet is upstream, facing into the uniform flow. From equations of the elementary flow of fluid mechanics and

the doublet (Anderson, 2007) $\Psi = V_\infty r \sin \theta$, $\Psi = -\frac{k}{2\pi} \frac{\cos \theta}{r}$ respectively, the stream function for the combined flow is

$$\Psi = V_\infty r \sin \theta - \frac{k}{2\pi} \frac{\cos \theta}{r} \quad (2.1)$$

or

$$\Psi = (V_\infty r \sin \theta) \left(1 - \frac{k}{2\pi V_\infty r^2}\right) \quad (2.2)$$

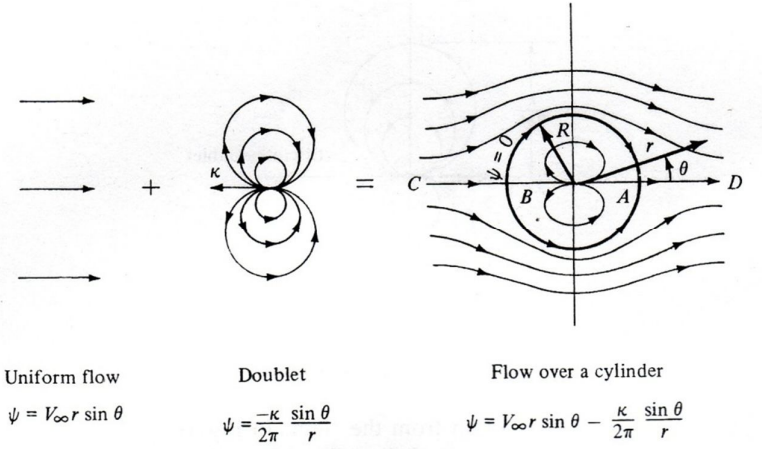


Figure 2.1 Superposition of a uniform flow and a doublet; nonlifting flow over a circular cylinder (Anderson, 2007)

Let $R^2 = \frac{k}{2\pi V_\infty}$. Thus the Equation (2.2) becomes

$$\Psi = (V_\infty r \sin \theta) \left(1 - \frac{R^2}{r^2}\right) \quad (2.3)$$

Equation (2.3) is the stream function for a uniform flow-doublet combination, also is the stream function for the flow over a circular cylinder of radius R. Continuing by differentiating the Equation (2.3) as follows:

$$V_r = \frac{1}{r} \frac{\partial \Psi}{\partial \theta} = \frac{1}{r} (V_\infty r \cos \theta) \left(1 - \frac{R^2}{r^2}\right) \quad (2.4)$$

$$V_r = (V_\infty \cos \theta) \left(1 - \frac{R^2}{r^2}\right) \quad (2.5)$$

$$V_\theta = -(V_\infty \sin \theta) \left(1 + \frac{R^2}{r^2}\right) \quad (2.6)$$

To locate stagnation points, setting Equations (2.5) and (2.6) equal to zero and solving them simultaneously for r and θ , we find that there are two stagnation points, located at $(r, \theta) = (R, 0)$ and (R, π) . These points are denoted as A and B, respectively as in Figure 2.1.

The velocity distribution on the surface of the cylinder is given by Equations (2.5) and (2.6), with $r=R$, resulting in

$$V_r = 0 \quad (2.7)$$

and

$$V_\theta = -2V_\infty \sin\theta \quad (2.8)$$

At the surface of the cylinder, V_r is geometrically normal to the surface, hence Equation (2.8) is consistent with the physical boundary condition that the component of velocity normal to a stationary solid surface must be zero.

The pressure coefficient C_{pi} is defined as

$$C_{pi} = \frac{p_i - p_\infty}{q_\infty} \quad (2.9)$$

where

$$q_\infty = \frac{1}{2} \rho_\infty V_\infty^2 \text{ (free stream dynamic pressure)}$$

p_i = pressure at tapping point i

p_∞ = static pressure of the free stream

For incompressible flow, C_p can be expressed in terms of velocity only. From Bernoulli's equation,

$$p_\infty + \frac{1}{2} \rho V_\infty^2 = p + \frac{1}{2} \rho V^2$$

or

$$p - p_\infty = \frac{1}{2} \rho (V_\infty^2 - V^2) \quad (2.10)$$

Substituting Equation (2.10) into Equation (2.9), we'll get

$$C_p = 1 - \left(\frac{V}{V_\infty} \right)^2 \quad (2.11)$$

Combination of Equations (2.8) and (2.11), the surface pressure distribution coefficient over a circular cylinder is

$$C_p = 1 - 4\sin^2\theta \quad (2.12)$$

It's observed that at the stagnation points $\theta = 0, \pi$ $C_p=1$. Also the maximum speed occurs at the top and bottom of the cylinder ($\theta = \frac{\pi}{2}, \frac{3\pi}{2}$) and the pressure coefficient there is -3.

Since the drag is more important than lift in this study, to calculate it the pressure distribution must be integrated. Let D be the drag per unit width acting in the x direction (Anderson, 2007). Integrating the component of the pressure force on an element $Rd\theta$ gives,

$$\begin{aligned} D &= \int_0^{2\pi} -pRd\theta \cos\theta = \int_0^{2\pi} -(p - p_\infty)Rd\theta \cos\theta \\ &= \frac{1}{2}\rho V_\infty^2 \int_0^{2\pi} (1 - 4\sin^2\theta)R\cos\theta d\theta = 0 \end{aligned} \quad (2.13)$$

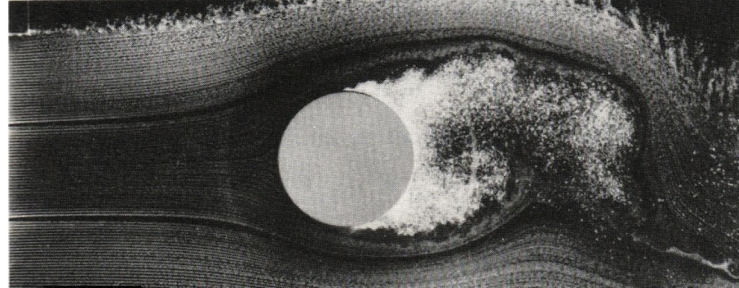


Figure 2.2 Hydrogen bubble visualization of the separated water flow around a cylinder at a Reynolds number of 0.2×10^6 (Courtesy of K.W.McAlister and L.W.Carr, U.S. Army Aeroflightdynamics Directorate, AVSCOM)

As mentioned before $C_p=1$ at $\theta = 0, \pi$. In reality the flow separates, and will not follow the cylinder's rear surface, as shown in Figure 2.2. The real pressure distribution along with the results from Equation (2.12), are plotted in Figure 2.3. This shows that at the front section of the cylinder, where the flow is attached, the pressures are well predicted by this model. However, behind the cylinder, due to the flow separation, the pressure distribution differs.

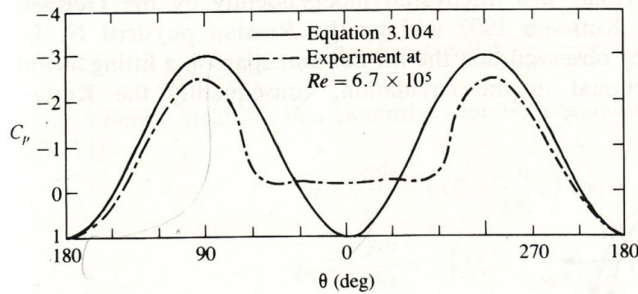


Figure 2.3 Theoretical pressure distribution (solid curve) around a cylinder compared with experimental data at Reynolds number of 6.7×10^5 (chain curve)
(Schlichting, 1979)

2.3 Flow field around a circular cylinder

Many factors characterize the flow around smooth cylinder in a disturbance-free flow. Usually Reynolds number is taken as a main parameter, defined as

$$Re = \frac{\rho V d}{\mu} \quad (2.14)$$

or replacing with kinematic viscosity

$$Re = \frac{V d}{\nu} \quad (2.15)$$

Where d is the diameter of the cylinder and ρ , V , ν and μ are the density, free stream velocity, kinematic and dynamic viscosities of the flow respectively.

Actually, Reynolds number stands for the ratio of inertial to viscous forces.

Schematic flow field around cylinder is shown in Figure 2.4. Reynolds number takes important place in transition of laminar flow to turbulent. These transitions play important role in affecting the drag coefficient.

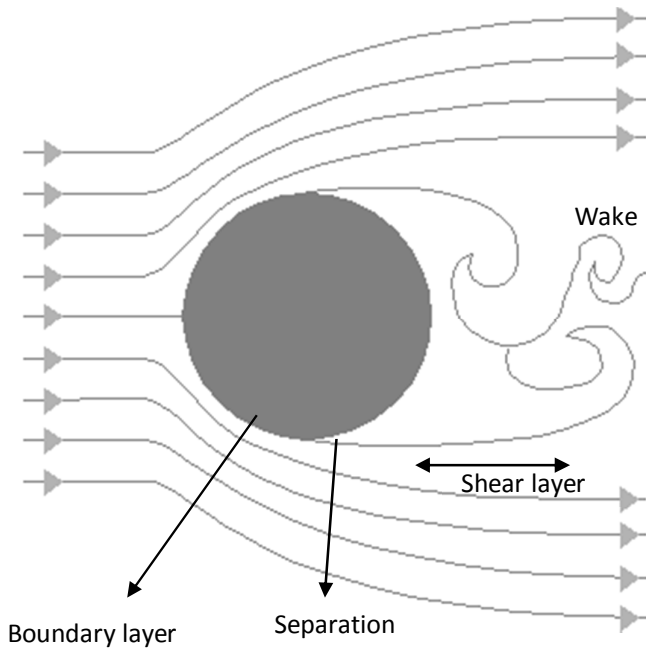


Figure 2.4 Flow field around circular cylinder

2.4 Drag coefficient of a circular cylinder

The drag data is presented in Figure 2.5, 2.6, 2.7 and Table 2.1 for circular cylinder as function of Reynolds number. According to Schlichting (p.17), for the laminar flows ($Re < 2000$) the drag is large owing to larger flow separation behind the body, which is being reduced as the turbulent flow momentum transfer increases ($Re > 10^5$). For the case of inviscid flow results do not include flow separation, and therefore the drag coefficient for cylinder is zero. This called d'Alambert's paradox.

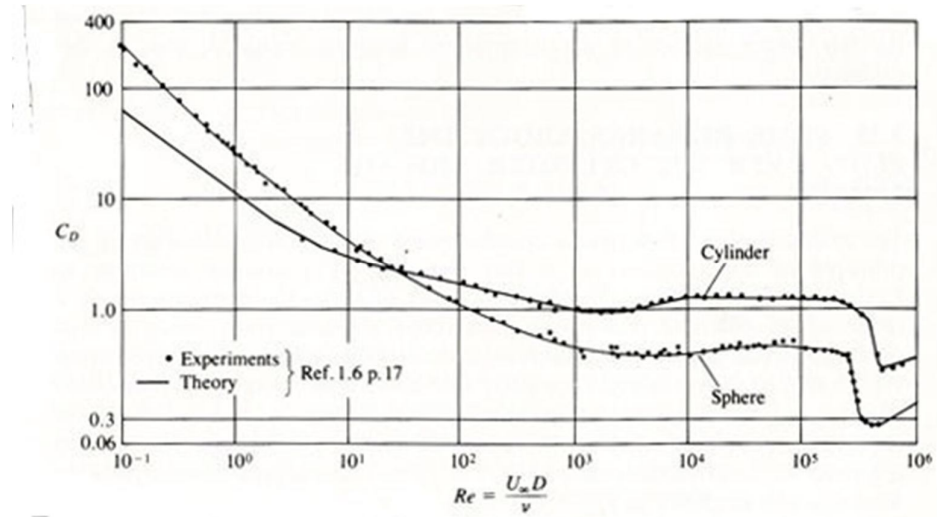


Figure 2.5 Typical experimental results for the drag coefficient for cylinders and spheres as function of Reynolds number(Schlichting, 1979)

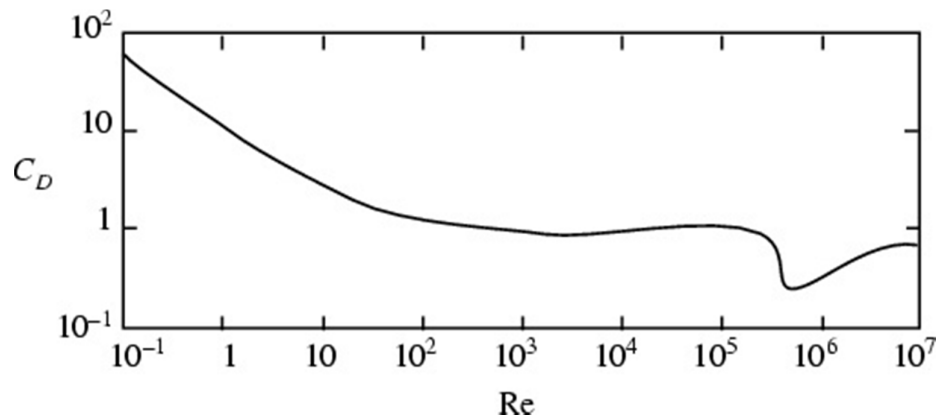


Figure 2.6 C_D vs. Re for infinite cylinder (Tritton,1988)

For an infinite circular cylinder of diameter d , the aerodynamic drag coefficient is expressed by

$$C_D = \frac{f_D}{\frac{1}{2}\rho V^2 d} \quad (2.16)$$

Where f_D is the drag force per unit length (Tritton 1988). Note that this definition replaces the F_D/d^2 present in the definition of the usual drag coefficient

with f_d/d .

According to Tritton (1988,pp 32-33) for $Re < 100$, $C_d \propto Re^{-1}$, for $100 < Re < 10^5$, $C_d \approx 1$, and for $Re > 3 \times 10^5$, C_D drops and then rises. The latter transition corresponds to the onset of turbulence in the boundary layer.

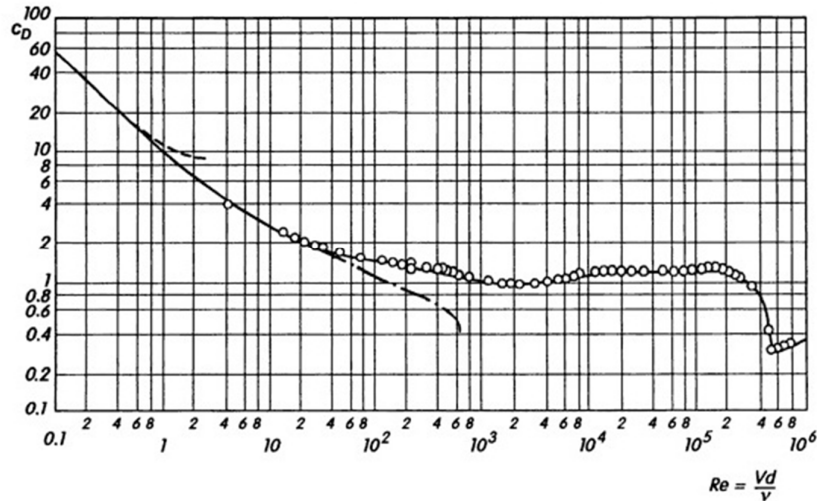


Figure 2.7 Circular cylinder: drag coefficient vs. Reynolds number

- measurements by C.Wieselberger
- — — asymptotic formula for $Re \rightarrow 0$, $C_d = \frac{8\pi}{Re} [\Delta - 0.87\Delta^3 + \dots]$
with $\Delta = \left[\ln \left(\frac{7.406}{Re} \right) \right]^{-1}$, $Re = \frac{Vd}{v}$, $C_d = \frac{2D}{\rho V^2 bd}$
- · — numerical results by A.E.Hamielec; J.D.Raal (1969) and B.Fornberg (1985) for steady flow

Table 2.1 relates Reynolds number to drag coefficient, flow form and flow regime. When Reynolds number near to zero, the flow is very steady, no wake occurs. While Reynolds number is approaching value about 30-40, steady symmetrical separation takes place, C_D range is 1.59-4.52. Next at Re up to 80-90 the flow is laminar, wake is unstable, C_D ranges from 1.17 to 1.59. Increasing Reynolds number to 300 produces Karman vortex sheet. Reynolds number up to 1.3×10^5 C_D is about constant having approximate value of 1.2. Then C_D drops and rises again. Laminar and turbulent separation occurs. Finally after the Reynolds number reaching values of 3.5×10^5 the C_D stay constant at 0.6, and turbulent separation takes place.

Table 2.1: Flow regimes at a circular cylinder (Schlichting, 1979)

Reynolds number	Flow regime	Flow form	Flow characteristics	C_D
$Re \rightarrow 0$	Creeping flow		Steady, no wake	-
$3-4 < Re < 30-40$	Vortex pairs in wake		Steady symmetrical separation	$1.59 < C_D < 4.52$ $Re = 30$ $Re = 40$
$30-40 < Re < 80-90$	Onset of Karman vortex sheet		Laminar, unstable wake	$1.17 < C_D < 1.59$ $Re = 100$ $Re = 30$
$80-90 < Re < 150-300$	Pure Karman vortex sheet		Karman vortex sheet	
$150-300 < Re < 10^5 - 1.3 \times 10^5$	Subcritical regime		Laminar with vortex street instabilities	$C_D \approx 1.2$
$10^5 - 1.3 \times 10^5 < Re < 3.5 \times 10^5$	Critical regime		Laminar separation, Turbulent reattachment, Turbulent separation, Turbulent wake	$0.2 < C_D < 1.2$
$3.5 \times 10^5 < Re$	Supercritical regime		Turbulent separation	$C_d \approx 0.6$

2.5 Transitions around a circular cylinder

The drag coefficient for the circular cylinder was well defined over different numbers of Re . Figure 2.8 presents C_D vs. Reynolds number, and shows flow transitions with Reynolds number changing. In this figure C_{df} and C_{dp} are the components of total drag force. Friction on the surface causes C_{df} , and not symmetrical pressure distribution on both sides of the cylinder causes C_{dp} . Zdravkovich suggested five flow transitions as shown in Figure 2.8. Starting from left to right, first region stands for a laminar flow. As marked in the Figure 2.8 the Reynolds number roughly less than 200. The next region is from $200 < Re < 400$, presents flow transition in the wake at the back side of the cylinder. By following at $Re=350 - 2 \times 10^5$ shear layer transition takes place. From $Re=3 \times 10^5$ to $Re=6 \times 10^6$ the transition in boundary layer occurs. As Reynolds number becoming higher, the flow becomes totally turbulent. Obviously in TrSL region as labeled in Figure 2.8, C_D is a constant and has value of 1.2, when Re from 10^4 to 2×10^5 . According to Zdravkovich, it's a subcritical region. Next, C_D drops quickly to 0.2 – 0.3 in the critical region. In this region C_D has minimum values. After Reynolds number greater than $3.5 \times 10^6 - 6 \times 10^6$, C_D can be assumed constant, and has values around 0.75 – 0.9. It's called supercritical region.

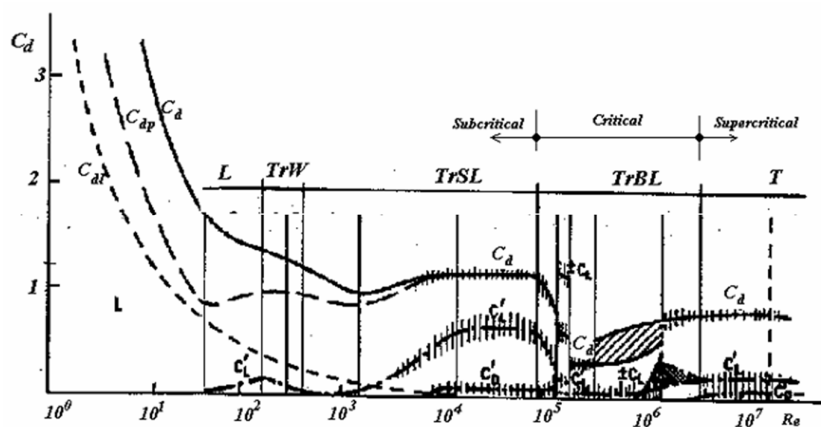


Figure 2.8 Variation of C_D and Flow Transitions for circular cylinder flow
(Zdravkovich, 1997)

2.6 Surface roughness effects

Aerodynamic drag coefficient differs with different surface roughness. Different roughness patterns produce different types of roughness, affecting the aerodynamics parameters. Suggestions were done by researchers in this area to adopt roughness parameter $\frac{K_s}{d}$. As shown in Figure 2.9, drag coefficient vs. Reynolds number at different roughness parameters.

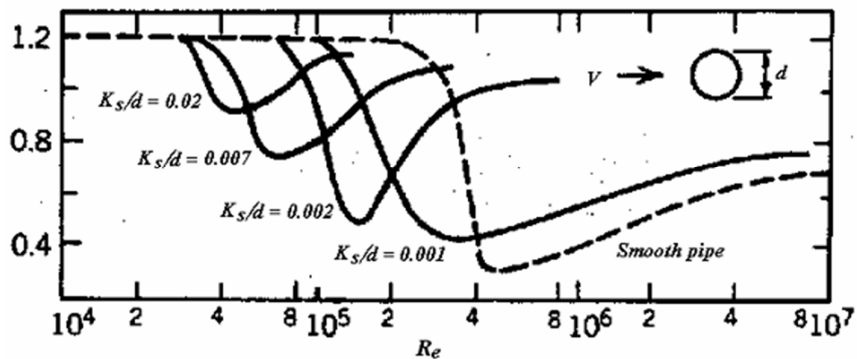


Figure 2.9 Effects of roughness parameter on drag coefficient (Zdravkovich)

Observation from above figure leads to that at Re lower than 3×10^4 the surface roughness do not affect the aerodynamic drag coefficient. Also increasing in roughness parameter will affect the Reynolds number in that way: values will be shifted to left, critical values of Re will have lower value.

2.7 Finite cylinder

All explained drag coefficients from theory and experiments were applicable to infinite cylinder. For cylinders of finite length with free ends, the drag coefficient

must be reduced using the data of Table 2.2. If a finite cylinder has one end fixed to a solid surface, the length of the cylinders is doubled (Merle C.Potter, D.C.Wiggert, 2007).

Table 2.2: Drag coefficients for finite-length circular cylinder with free ends

L/D	$C_D/C_{D\infty}$
∞	1
40	0.82
20	0.76
10	0.68
5	0.62
3	0.62
2	0.57
1	0.53

2.8 Boundary corrections of wind tunnel data

The existence of wind tunnel walls confining the flow around a model in the test section reduces the area through which air must flow as compared to free-air conditions and applying continuity and Bernoulli's equations, increases the velocity of the air as it flows in the vicinity of the model. This increase of velocity, which is approximated as constant over the model, is called solid blockage. Its effect is a function of model thickness, thickness distribution, and model size and is independent of camber.

Now consider solid blockage for a circular cylinder in a two-dimensional tunnel. The cylinder simulated by a doublet of strength $k = 2\pi Vr^2$, where r is a radius of a cylinder (Barlow, 1999). Taking the vertical series of doublets of the same strength as the one simulating model, the axial velocity of the first doublet is

$$\Delta V = \frac{k}{2\pi h^2} \quad (2.17)$$

so that

$$\frac{\Delta V}{V_u} = \frac{r^2}{h^2} \quad (2.18)$$

where V_u is uncorrected velocity.

Since the velocity produced by a doublet varies inversely with the square of the distance from the doublet, the two sided infinite series may be summed as

$$\begin{aligned} \varepsilon &= \left(\frac{\Delta V}{V_u} \right)_{total} = 2 \sum_1^\infty \frac{1}{n^2} \frac{r^2}{h^2} \\ &= \frac{\pi^2 r^2}{3h^2} \end{aligned} \quad (2.19)$$

The solid-blockage corrections for three-dimensional case follow the same principles as for two-dimensional flow. According to Herriot, the body represented by a source-sink distribution and is contained in the tunnel walls by an infinite distribution of images. Summing up the effect of the images, for solid-blockage velocity effect for a cylinder

$$\varepsilon = \frac{\pi r^2}{3h^2} \tau_1 \quad (2.20)$$

where τ_1 is a factor depending on the tunnel test-section shape and the model span-to-tunnel width ratio. The values for τ_1 are presented in Figure 2.11.

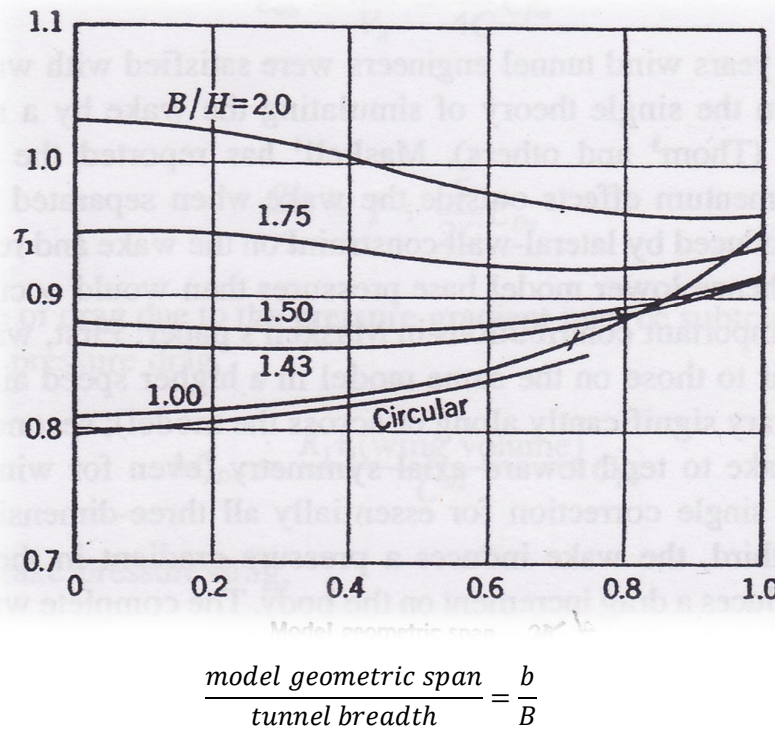


Figure 2.10 Values of τ_1 for a number of tunnel types (Barlow, 1999)

2.9 Computational fluid dynamics

2.9.1 Equation describing flow

In mid-18th century, the French engineer Claude Navier and the Irish mathematician George Stokes derived the well-known equations of fluid motion, known as the Navier-Stokes equations. These equations have been derived based on the fundamental governing equations of fluid dynamics, called the continuity, the momentum and the energy equations, which represent the conservation laws of physics.

Continuity equation based on the law of conservation of mass. Applying this concept to fluid flow, we ensure that the change of mass in a control volume is equal to the mass that enters through its faces minus the total mass leaving its faces.

By applying Newton's Second Law of Motion, the momentum equation is expressed in terms of the pressure and viscous stresses acting on a particle in the fluid. This ensures that the rate of change of momentum of the fluid particles is equal to the total force due to surface stresses and body forces acting in an aligned direction of a chosen coordinate axis.

Energy equation based on the First Law of Thermodynamics, the rate of change of energy of a fluid particle is taken to be equal to the net rate of work done on that particle due to surface forces, heat and body forces such as gravitational force. The energy equation describes the transport of heat energy through a fluid and its effects.

2.9.2 Navier-Stokes equations

Combining these fundamental principles, the physics of fluid flow is expressed in terms of a set of partial differential equations known as the Navier-Stokes equations. By solving these equations, the pressure and velocity of the fluid can be predicted throughout the flow (Versteeg H.K., Malalasekera W., 1995). Assuming that the flow is incompressible, the following equations can be used to describe the fluid flow, Navier-Stokes Equations: (conservation of momentum),

$$\frac{\partial u_i}{\partial t} + u_j \frac{\partial u_i}{\partial x_j} = -\frac{1}{\rho} \frac{\partial p}{\partial x_i} + \frac{\partial}{\partial x_j} \left(\nu \frac{\partial u_i}{\partial x_j} \right) \quad (2.21)$$

The continuity equation: (conservation of mass),

$$\frac{\partial u_i}{\partial x_j} = 0 \quad (2.22)$$

where u is the velocity in the stream wise direction, p is the pressure, ρ is the fluid density and ν is the kinematic viscosity of the flow.

2.9.3 Turbulence models

Turbulence modeling is the construction and use of a model to predict the effects of turbulence. Averaging is often used to simplify the solution of the governing equations of turbulence, but models are needed to represent scales of the flow that are not resolved (Ching Jen Chen, Shenq-Yuh Jaw, 1998).

Reynolds-Averaged Navier-Stokes (RANS) models solves time-averaged Navier-Stokes equations.

According to ANSYS Fluent helping notes, turbulence models are sorted in ascending order of computational cost per iteration as follow: Spalart-Allmaras, Standard $k-\epsilon$, RNG $k-\epsilon$, Realizable $k-\epsilon$, Standard $k - \omega$, SST $k - \omega$.

2.9.3.1 The $k-e$ Turbulence Model

Specifications

- The most widely-used engineering turbulence model for industrial applications
- Robust and reasonably accurate
- Contains submodels for compressibility, buoyancy, combustion, etc.

Limitations

- The ϵ equation contains a term which cannot be calculated at the wall. Therefore, wall functions must be used.
- Generally performs poorly for flows with strong separation, large streamline curvature, and large pressure gradient.

2.9.3.2 Realizable k-e model

The term realizable means that the model satisfies certain mathematical constraints on the Reynolds stresses, consistent with the physics of turbulent flows.

Benefits:

- More accurately predicts the spreading rate of both planar and round jets.
- Also likely to provide superior performance for flows involving rotation, boundary layers under strong adverse pressure gradients, separation, and recirculation.

2.9.4 Mesh statistics

2.9.4.1 Skewness

In probability theory and statistics, skewness is a measure of the asymmetry of the probability distribution of a real-valued random variable.

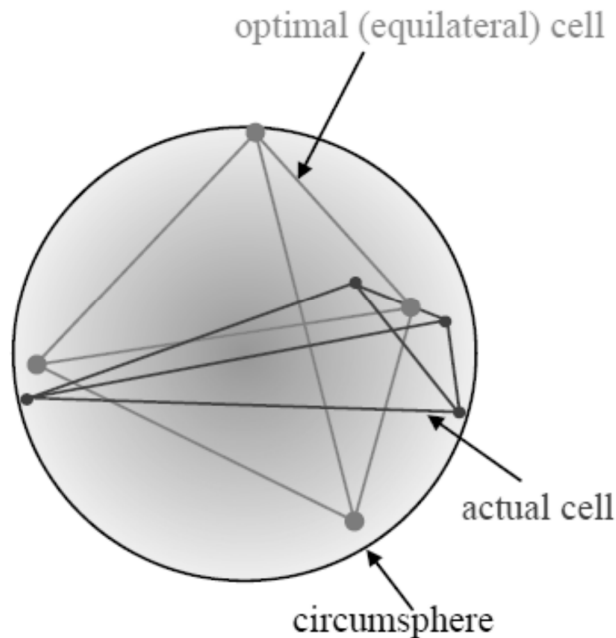


Figure 2.11 Skewness in meshing (Fluent helping notes)

The formula to calculate skewness:

$$\text{skewness} = \frac{\text{optimal cell size} - \text{cell size}}{\text{optimal cell size}} \quad (2.23)$$

The Equation above applies only to triangular and tetrahedral structures. The value varies from 0 to 1. The lowest values are preferable.

Acceptable values for skewness in CFD (Fluent helping notes)

- For Hexa, Tri and Quad: it should be less than 0.8
- For tetrahedral it should be less than 0.9

2.9.4.2 Aspect ratio

Aspect for generic triangles and quads is a function of the ratio of longest side to the shortest side of the reconstructed quadrangles

- It should be less than 40, but this depends on the flow characteristics
- More than 50 may be tolerated at the inflation layers

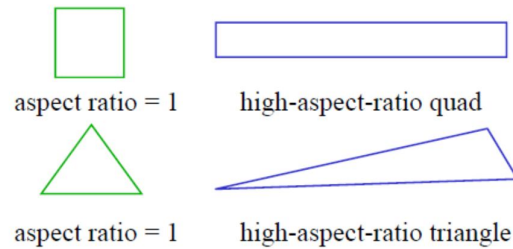


Figure 2.12 Aspect ratio in meshing (Fluent helping notes)

CHAPTER 3

APPARATUS AND SOFTWARE

3.1 Wind tunnel

3.1.1 Introduction

A wind tunnel is the tool that has airflow produced by fans, with test section with an object inside. This can be anything, aircraft, car or other object that needs to be measured for specific parameters such as drag coefficient, lift or pressure distribution. The object inside test section never moves, airflow created by fans is flowing towards the tested object. This is the same as objects moves through the airflow. The wind tunnels equipped with computers and control room. With computer aid all the needed parameters can be obtained. Sometimes smoke is used to create flow visualization.

There are two basic types of wind tunnels and two basic test-section configurations. However, there are almost endless variations on the specific features of various tunnels. The two basic types are open circuit and closed circuit. The two basic test-section configurations are open test section and closed test section.

The air flowing through an open circuit tunnel follows an essentially straight path from the entrance through a contraction to the test section, followed by diffuser,

a fan section, and an exhaust of the air. The tunnel may have a test section with no solid boundaries (open jet or Eiffel type) or solid boundaries (closed jet or National Physical Laboratory (NPL) type). Figure 3.1 shows a plan view of an open circuit tunnel with a closed jet.

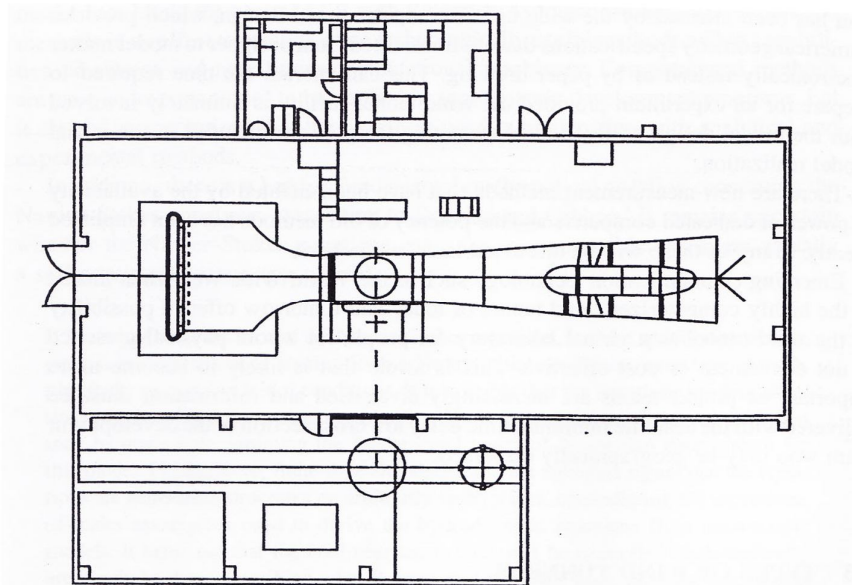


Figure 3.1 Plan view of an open circuit wind tunnel (Diamler-Benz Aerospace
Airbus, Bremen, Germany)

The air flowing in a closed return wind tunnel, Prandtl, or Gottingen type, recirculates continuously with little or no exchange of air with exterior. A schematic drawing of a closed circuit tunnel is shown in Figure 3.2.

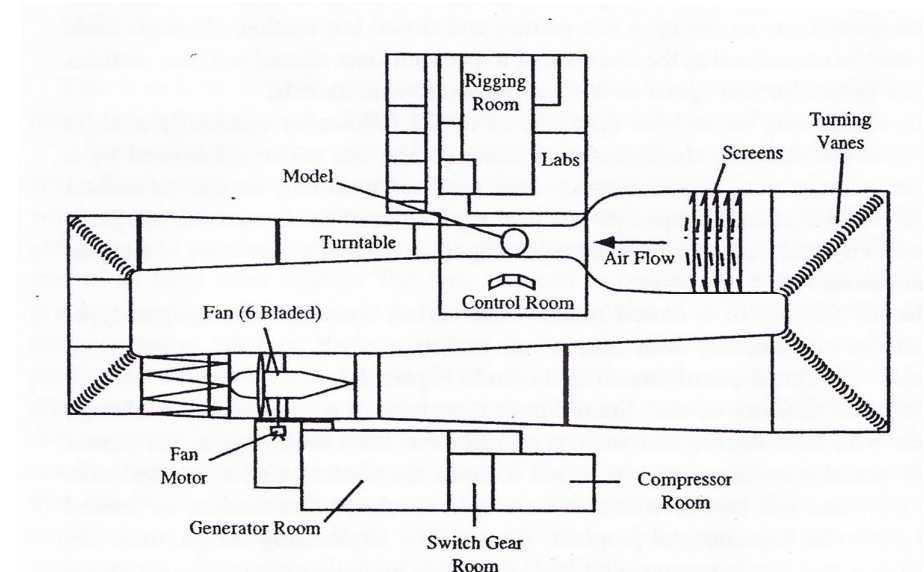


Figure 3.2 A closed circuit wind tunnel, (DERA), 13x9-ft tunnel in Bedford, England

The great majority of the closed circuits tunnels have a single return. The closed circuit tunnel may have either a closed or open test section, and a number have been built that can be run with either an open or closed test section, as needed for a particular experiment. There are advantages and disadvantages with both the open- and closed-circuit type tunnels and with both open and closed jets.

The following are advantages and disadvantages of a closed return tunnel:

Advantages

1. Corners turning vanes and screens gives well control on the quality of the flow, and will be independent of other activities in the building and weather conditions.
2. Less energy is required for a given test-section size and velocity.
3. Less environmental noise while operating.

Disadvantages

1. The initial cost is higher compared to open return wind tunnels.
2. If used extensively for smoke flow visualization experiments or running of internal combustion engines, there must be a way to purge tunnel.
3. If tunnel has high utilization, it may have to have an air exchanger or some other method of cooling.

3.1.2 UTM Wind Tunnel

Aeronautical Laboratory is a specialized laboratory and a center of excellence in Universiti Teknologi Malaysia. The main laboratory facility is the Low Speed Wind Tunnel of 2.0m x 1.5m test section and maximum speed wind speed of 80 m/s with excellent flow quality and presented in Figure 2.10. This facility, the first of its kind in Malaysia, became operational in June 2001 and now is ready to contribute significantly to the technology development in aircraft design and aerospace fields. It is closed circuit wind tunnel.

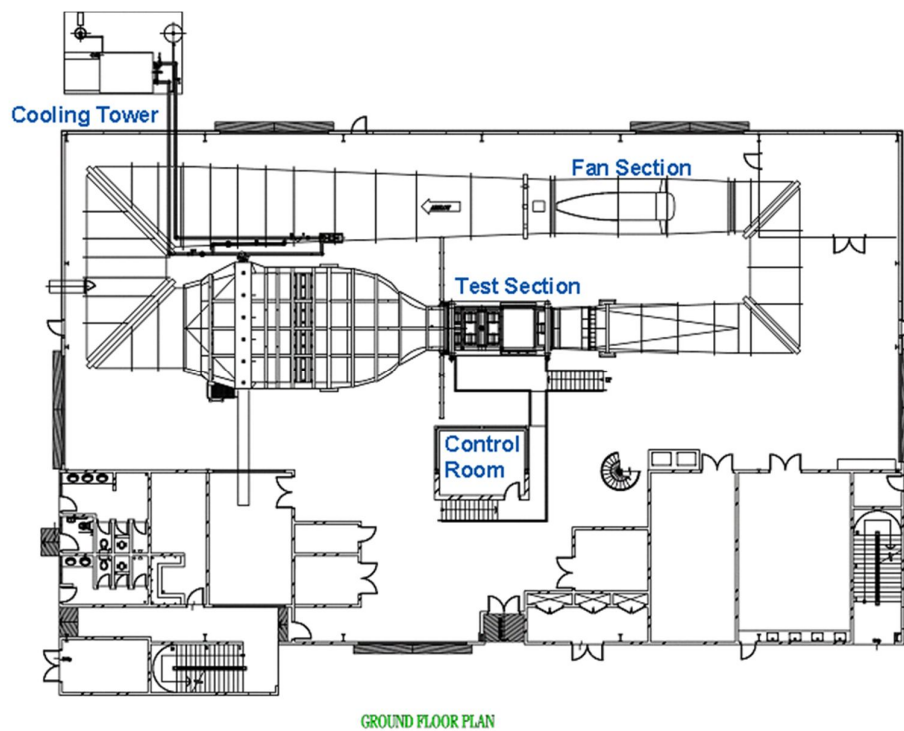


Figure 3.3 Plan of UTM Low-Speed Wind Tunnel Facility

Basic technical data of UTM Low-Speed Wind Tunnel.

Circuit

- Closed-return type
- Contraction ratio 9:1
- Heat exchanger system
- 430 kW AC motor, Axial fan

Test section

- 2.0m (W) x 1.5m (H) x 5.8m (L), solid walls
- Maximum wind speed 80 m/s (Mach 0.23)
- Atmospheric, interchangeable test section

Flow quality

- Velocity Uniformity <0.15%
- Temperature Uniformity <0.2 °C
- Flow angle Uniformity <0.15°
- Turbulence <0.06%

Facility Control system

- Fully integrated automatic computer Control and Data Acquisition System
- Mode of Operation – Pre-test, Test execution, Post Test Analysis, Calibration
- Pacific Instrument PI 6000 series Data Acquisition System
- Windows 2000 Operating System

Test Equipment & Instrumentation

- 6-Component External balance
- Underfloor turntable
- 3-point Strut Support System
- Pitch and Yaw capabilities
- Internal balance (automotive)
- Half-Model balance
- 128-port Electronic Pressure Scanning system
- Probe Traversing System for flow field survey
- Dual Channel Hotwire system
- Flow Visualization (Laser sheet & Smoke generator)

Accuracy to fullscale is 0.04%.

3.2 Drag Measurement

All loads on objects in wind tunnel are resolved in six components using 6-component external balance equipment. The balance load range and wind tunnel balance of UTM wind tunnel is presented in Table 3.1 and Figure 3.4 respectively.

Table 3.1: Balance load range

	6-Component External Balance
Normal Force, F_z	+/- 4500 N
Axial Force, F_x	+/- 1200 N
Side Force, F_y	+/- 1200 N
Pitching Moment, M_y	+/- 450 Nm
Yawing Moment, M_z	+/- 450 Nm
Rolling Moment, M_x	+/- 450 Nm
Primary Accuracy	< 0.04% FS

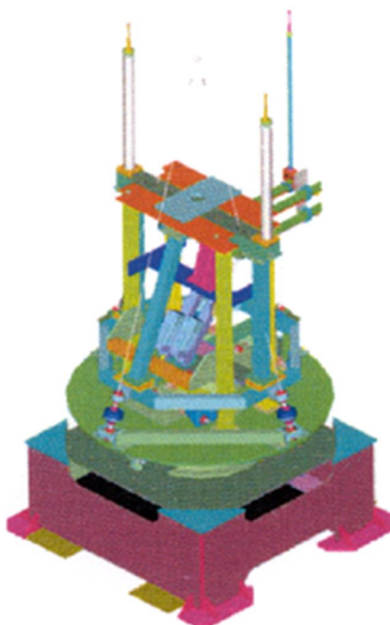


Figure 3.4 Wind tunnel balance

3.3 Software

3.3.1 Introduction to ANSYS

ANSYS FLUENT is a computational fluid dynamics (CFD) software package to simulate fluid flow problems. It uses the finite-volume method to solve the governing equations for a fluid. It provides the capability to use different physical models such as incompressible or compressible, inviscid or viscous, laminar or turbulent, etc.

3.3.2 Computational fluid dynamics

Computational fluid dynamics (CFD) solves the Navier-Stokes Equations numerically for fluid flow using computers. All CFD codes contain three main elements: the pre-processor, the solver and the postprocessor.

Pre-processor: employed to fully specify a CFD flow problem in a form suitable for the use of the solver. The region of fluid to be analyzed is called the computational domain and it is made up of a number of discrete elements called the mesh. The users need to define the properties of fluid acting on the domain before the analysis is begun; these include external constraints or boundary conditions, like pressure and velocity to implement realistic situations.

Solver: a program that calculates the solution of the CFD problem. Here the governing equations are solved. This is usually done iteratively to compute the flow parameters of the fluid as time elapses. Convergence is important to produce an accurate solution of the partial differential equations.

Post-processor: used to visualize and quantitatively process the results from the solver. In a contemporary CFD package, the analyzed flow phenomena can be

presented in vector plots or contour plots to display the trends of velocity, pressure, kinetic energy and other properties of the flow.

Nowadays, computer technology gives ability to enable CFD to be applied to complex flows and geometries and has become an essential tool in applications on wind engineering study. In CFD study, another aspect of consideration of a simulation is the residuals of the solutions. The equations describing fluid flow are solved iteratively so residuals appear. In engineering application, a residual is usually targeted between four to six orders of magnitude of the actual values (Stangroom, 2001) to achieve convergence of the solution to an acceptable level.

CHAPTER 4

METHODOLOGY

4.1 Introduction

This study aims to determine the aerodynamics drag coefficient of different sizes of cylinder by conducting wind tunnel test and simulation approach. The models will be in four different sizes. The test also will be conducted at four different wind speeds to investigate the Reynolds number effects. Different size in this study implies difference in diameter only, while keeping length of cylinder constant.

4.2 Experimental setup

Four different sizes for cylinder are used to investigate the effect of cylinder size on aerodynamic drag coefficient. Investigation includes analysis C_D vs. diameter of the cylinder and Reynolds number. The aim of the investigation is size effect on drag coefficient at different speeds. In this study, changing in size is changing in diameter only. For testing purpose four different speeds and diameters were chosen

to run the experiment and simulation. The main reason of choosing four different speeds and sizes is to plot graphs, and to have more data to compare results. The testing wind speed and diameter of cylinders were chosen as follows respectively: 10m/s, 20m/s, 30m/s and 40m/s; 32mm, 50mm, 65mm and 75mm. Recall Equation 2.14 and substituting values will give Reynolds numbers at different speeds and sizes. Here is the example of calculation of Reynolds number at 10 m/s with 32mm diameter:

$$Re = \frac{1.17 \times 10 \times 0.032}{1.86 \times 10^{-5}} = 2.013 \times 10^4$$

Similarly, for remaining diameter and testing speeds Reynolds number was calculated and tabulated in Table 4.1.

Table 4.1: Reynolds number at different speed with different diameter

Wind speed (m/s)\D(mm)	10	20	30	40
32	2.013×10^4	4.026×10^4	6.039×10^4	8.052×10^4
50	3.145×10^4	6.290×10^4	9.435×10^4	1.258×10^5
65	4.089×10^4	8.177×10^4	1.227×10^5	1.635×10^5
75	4.717×10^4	9.435×10^4	1.415×10^5	1.887×10^5

4.3 Wind tunnel testing

The wind tunnel testing will be conducted for four circular cylinders at different testing speed. The drag coefficient will be obtained from wind tunnel testing will be compared with CFD results and results were presented in Chapter 2. The tested model will be placed in the test section as follows:

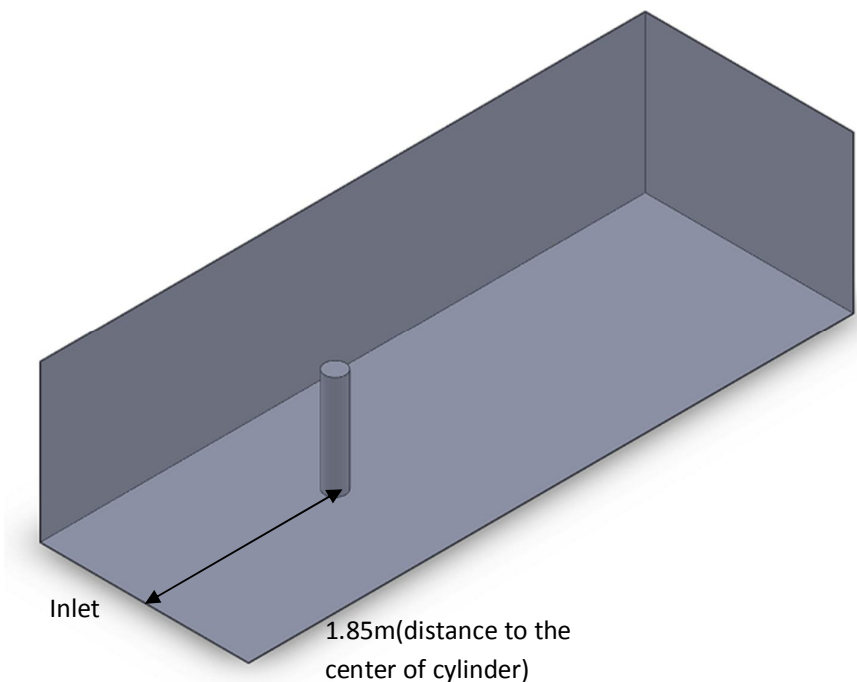


Figure 4.1 Placement of cylinder in the test section

4.4 Testing models

Four aluminum circular cylinders will be requested from store in university. The diameters for models are 32, 50, 65 and 75 mm. The surface of aluminum models will be washed in order to make surface as smooth as possible. The flowchart for wind tunnel testing is presented in Figure 4.2. First tone reading will be done for each cylinder, and then speed will be setup to 10, 20, 30 and 40 m/s. For each run 100 data will be recorded. Drag force will be calculated by subtracting average values of tone reading from wind speed reading. After the values of drag force will be calculated, drag coefficient can be found using Equation 2.16. Corrections no need to be carried out, since the largest cylinder front area is much less than 10% of wind tunnel section area.

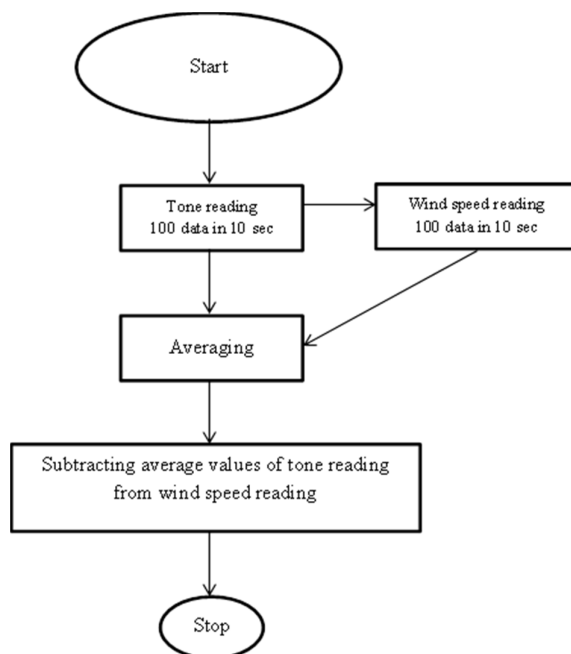


Figure 4.2 Flowchart for experiment

4.5 Computational Fluid Dynamics (CFD)

The CFD software used in this study is ANSYS 12.0. This software includes all the three major components of the analysis which is design modeling, meshing and solver. The solver used in ANSYS 12.0 is ANSYS FLUENT 12.0. ANSYS FLUENT 12.0 has extensive range of physical modeling capabilities. It has been successfully applied to industrial applications ranging from flow over an aircraft wing to combustion in furnace. Some of the functions provided by ANSYS Fluent 12.0 are:

- i. Turbulence: The range of turbulence option and the ability for further customization help to simulate turbulence for any flow condition. There are several popular turbulent models available in this software like k-epsilon and k-omega.
- ii. Acoustics: Analysis of noise from the source ranging from exposed bluff bodies to rotating fan blades.
- iii. Dynamic and moving mesh: Allows engineers to model the arbitrary, complicated motion of parts in challenging applications such as internal combustion engines, valves and rocket launchers.
- iv. Heat transfer, phase changing and radiation: it has a comprehensive suite of options for modeling convection, conduction and radiation. Other applications that can be solved by using this software are cavitation, compressible liquids, and heat exchangers.
- v. Reacting flow: modeling of chemical reactions especially in turbulent conditions. The eddy dissipation, equilibrium mixture fraction and other related reactions can be simulated in this software.

Since ANSYS 12.0 contain all two main requirement for a CFD software which Meshing and Fluent, there is no need for other software. The flowchart for the CFD simulation given in Figure 4.2:

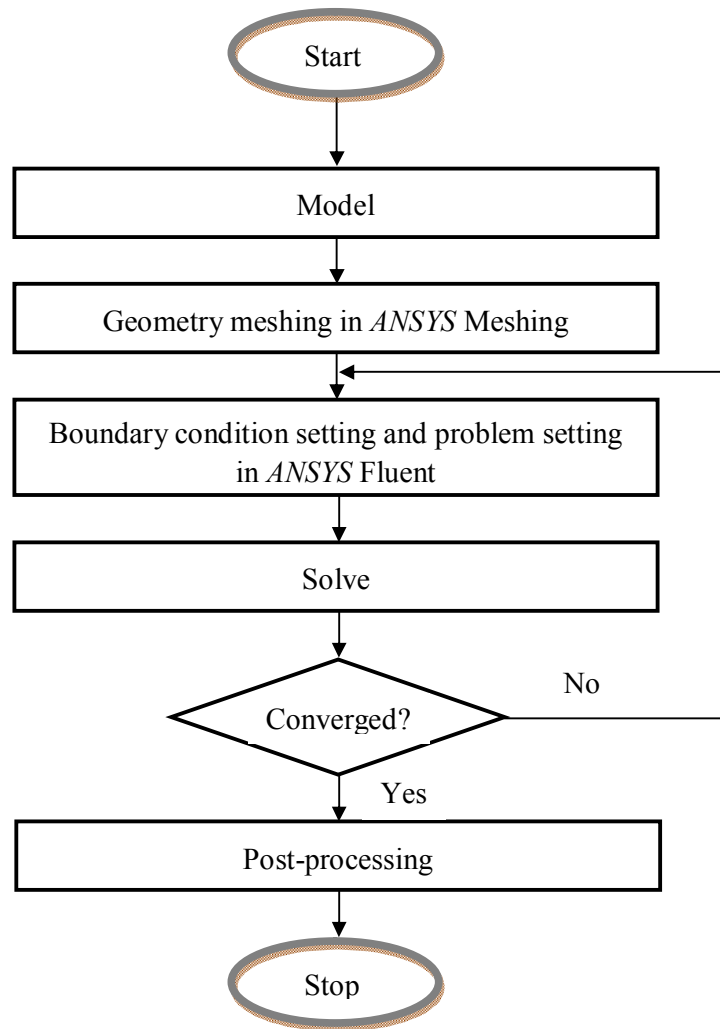


Figure 4.3 Flowchart for CFD simulation

4.5.1 Geometry

The cylinder was created at 1.85m distance from inlet. Domain has UTM wind tunnel's dimensions as follow: 2 m in width, 1.5m in height and 5.8m in length as shown in Figure 4.3.

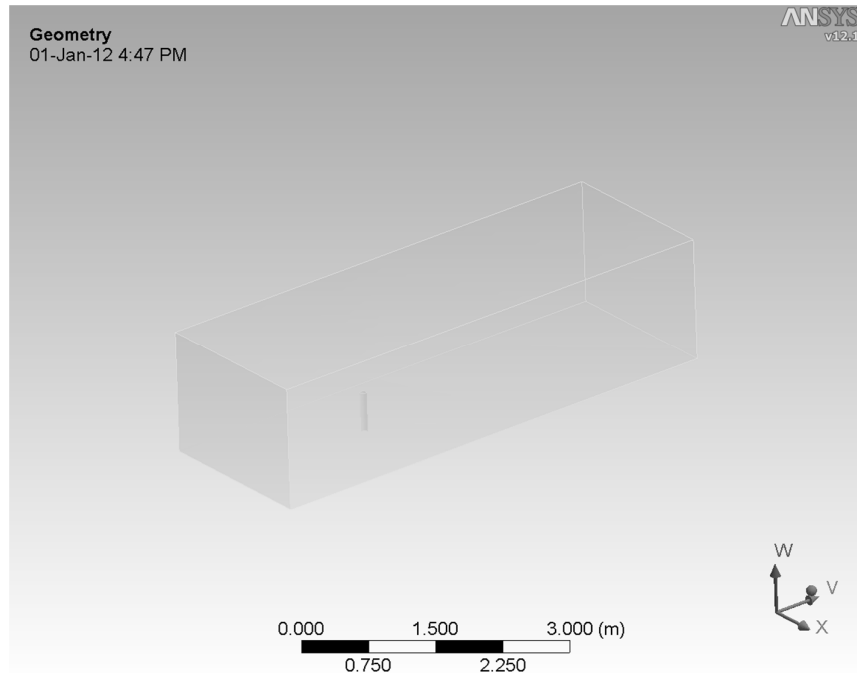


Figure 4.4 Geometry

4.5.2 Meshing

Tetrahedrons method with patch independent was chosen as the main meshing method due to:

- Faces and their boundaries (edges and vertices) are not necessarily respected unless there is a load, boundary condition, or other object scoped to them
- Useful for gross featuring or to produce a more uniformly sized mesh
- Tetra parts can also have inflation applied

Inflation is used to make more uniform elements around cylinder. It is accomplished by extruding faces normal to a boundary to increase the boundary resolution and gives smooth transition from inflated layer to interior mesh. Face sizing is used for cylinder part. It gives more elements on cylinder's surface. All meshing methods described are shown in Appendix A-C.

4.5.3 Boundary conditions

All faces in domain will be named as appropriate boundary conditions. For inlet, inlet velocity will be the input parameter, although for outlet it will be the pressure. All walls are selected to free slip walls, and doesn't have specific shear.

4.5.4 Turbulence model

For turbulence model, realizable k-e model is chosen since it has enough accuracy to model the flow with specific conditions. In this case it is cylinder in wind tunnel test. The geometry is not complex, flow doesn't have swirling particles, and the flow is steady.

4.5.5 Fluent analysis

The simulation in CFD will be run for different models in three dimensional analyses. The variable that will be changed for tested model is the velocity of the wind. Four different speeds are 10m/s, 20 m/s, 30m/s and 40 m/s.

4.5.6 Post-processing

After solving the problem with fluent, the results will be shown in post-processing of data. The post-processing is the presentation of results. The results will be presented in different methods like contours, graphs, streamline and others. In this study the interested is the drag force and coefficient.

CHAPTER 5

RESULTS AND DISCUSSION

5.1 Introduction

In previous chapters, theory about flow around a circular cylinder, apparatus and software used, methods and steps to do the experiment and to run simulation were briefly discussed. Experiment was performed in UTM wind tunnel, simulation was conducted using ANSYS software. This chapter will be discussed about results of experiment and simulation works.

5.2 Experimental results

Each cylinder was tested in wind tunnel at four different speeds. The axial force acting on cylinder was recorded during the test for ten seconds for each speed. Average value was taken as a drag force value. Results presented in Table 5.1 as a drag force and drag coefficient for each cylinder at different speeds. Drag coefficient was calculated using Equation 2.16:

$$C_D = \frac{F}{\frac{1}{2}\rho V^2 A}$$

where F is the axial force in flow direction, A is the projected area of the cylinder exposed to the flow, ρ and V is the density and free stream velocity of the flow respectively. Projected area is calculated by multiplying length with diameter of the cylinder.

Table 5.1: Results from experiment

	Size1(32mm)				Size2(50mm)			
Wind speed (m/s)	10	20	30	40	10	20	30	40
Drag force (N)	0.86	2.69	5.22	8.49	1.26	3.74	7.53	13.00
Drag coefficient	0.92	0.72	0.62	0.57	0.86	0.64	0.57	0.56
	Size3(65mm)				Size4(75mm)			
Wind speed (m/s)	10	20	30	40	10	20	30	40
Drag force (N)	1.54	4.55	9.04	16.47	1.77	4.64	11.24	20.13
Drag coefficient	0.81	0.60	0.53	0.54	0.81	0.53	0.57	0.57

Drag force was plotted versus wind speed and presented in Figures 5.1. In addition, drag coefficient was plotted versus wind speed in Figure 5.2. Reynolds number was calculated using Equation 2.14, as presented by

$$Re = \frac{\rho V d}{\mu}$$

where d is a diameter of the cylinder, ρ, V, μ are density, free stream velocity, and dynamic viscosity of the flow respectively. The diameter and velocity is changing, but density and dynamic viscosity are remaining constant and have values of 1.17 and 1.86×10^{-5} respectively. All sizes were presented in one graph, so they can be easily compared.

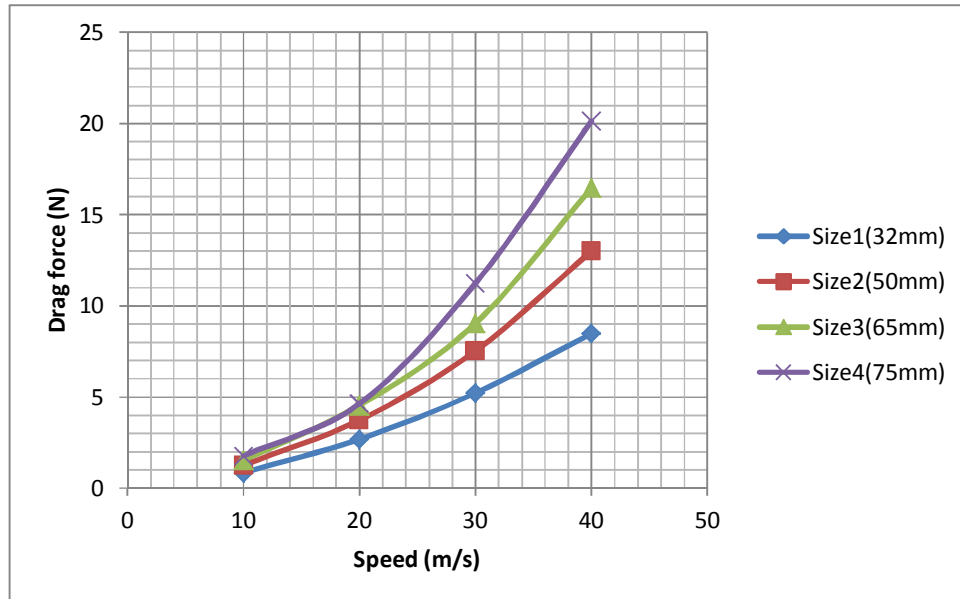


Figure 5.1 Drag force versus wind speed

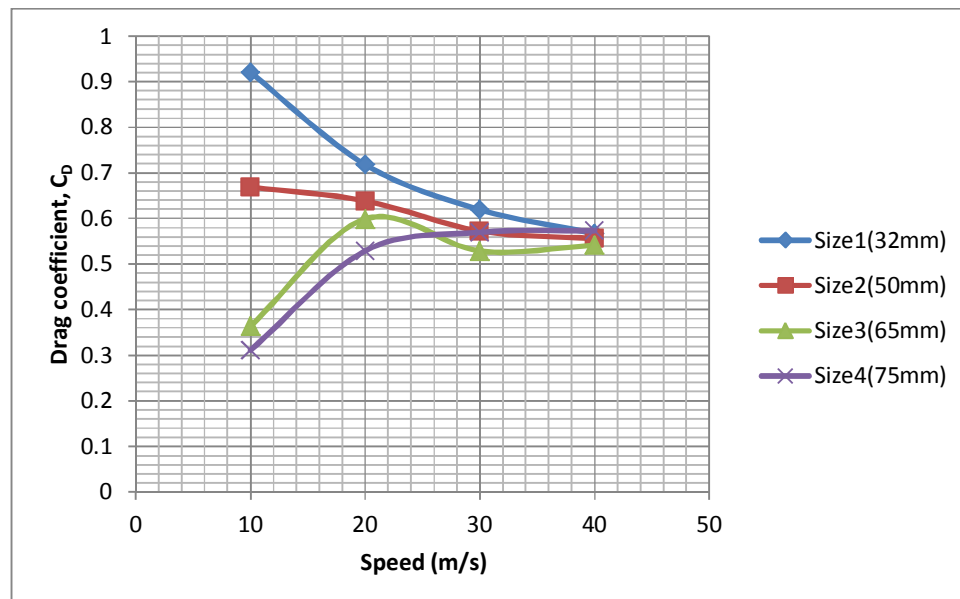


Figure 5.2 Drag coefficient versus wind speed

Graphs in Figure 5.3 and 5.4, shows drag force and drag coefficient versus size, in this study it is a diameter. Data was plotted at different wind speeds.

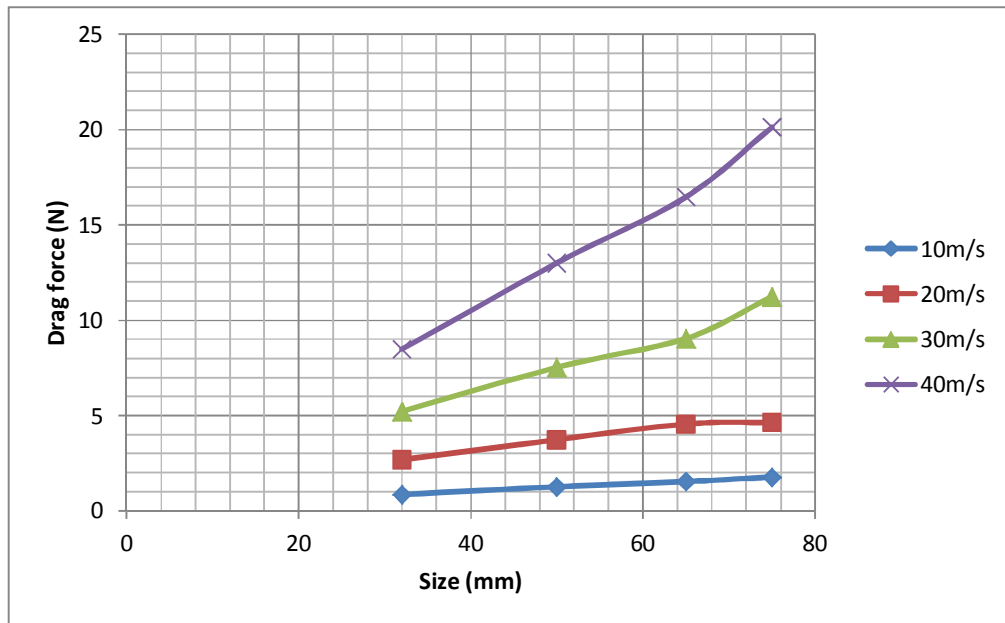


Figure 5.3 Drag force versus diameter

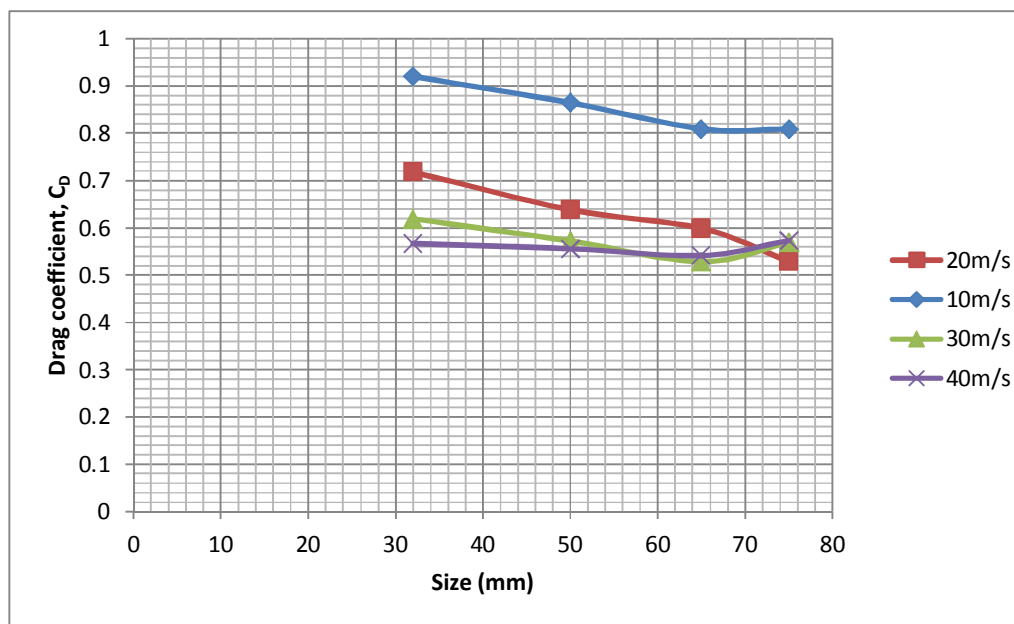


Figure 5.4 Drag coefficient versus diameter

5.3 Verification of the results

Drag coefficient was plotted versus Reynolds number for experimental, theoretical and simulation results to verify the results at different wind speeds. Theoretical values were taken from Chapter 2, according to Schlichting, 1979. However, these values are for infinite cylinder. To make values comparable, Table 2.2 is used to convert drag coefficient from infinite cylinder to finite. Length for cylinder is 0.5 m, and diameter for size 2 is 0.05 m. It brings L/D to 10. For this value of L/D , $C_D/C_{D\infty}$ is 0.68. That means the values of drag coefficient for infinite cylinder should be multiplied by 0.68. Drag coefficient for 50mm cylinder at 10m/s is 1.2, so multiplying by 0.68 results 0.816. From experiment drag coefficient was 0.86. In similar way drag coefficients was calculated and compared with experimental results. The graphs are presented in Figure 5.5, 5.6, 5.7 and 5.8. Graphs show that values of drag coefficient are very close to each other and agreeable.

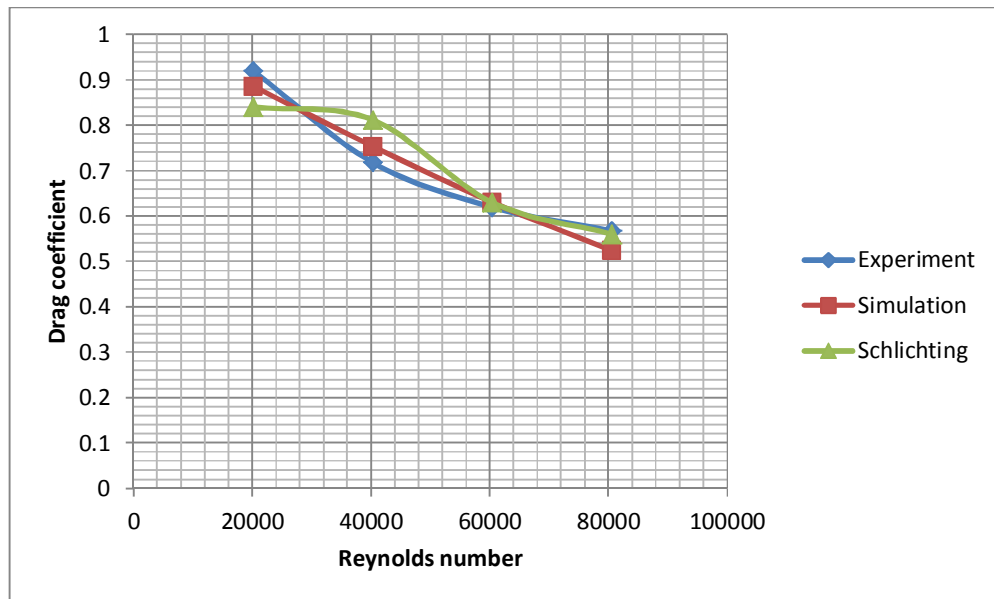


Figure 5.5 Drag coefficient versus Reynolds number (32mm)

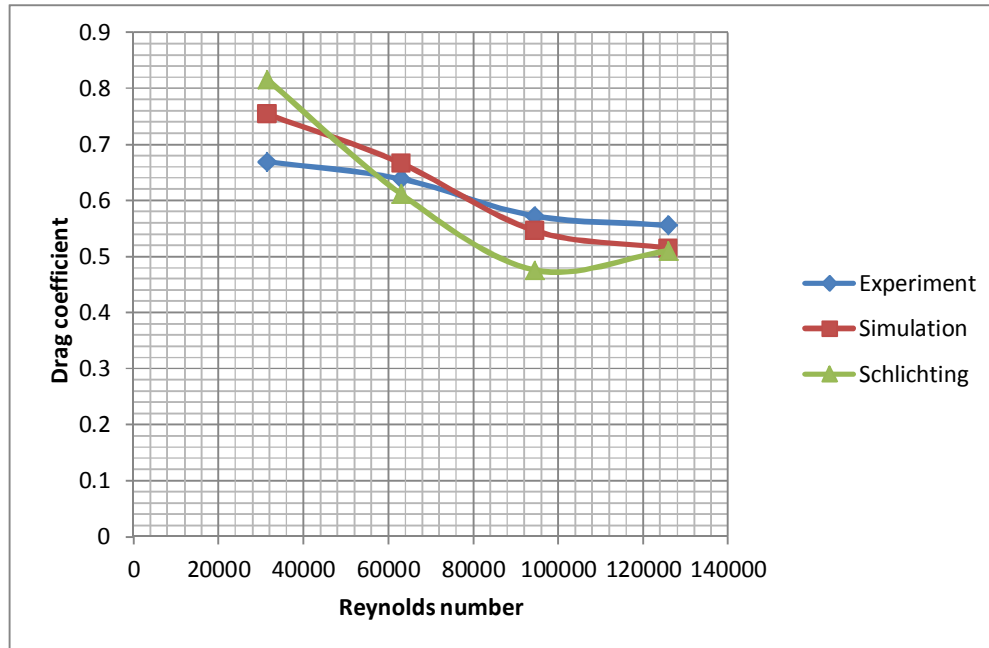


Figure 5.6 Drag coefficient versus Reynolds number (50mm)

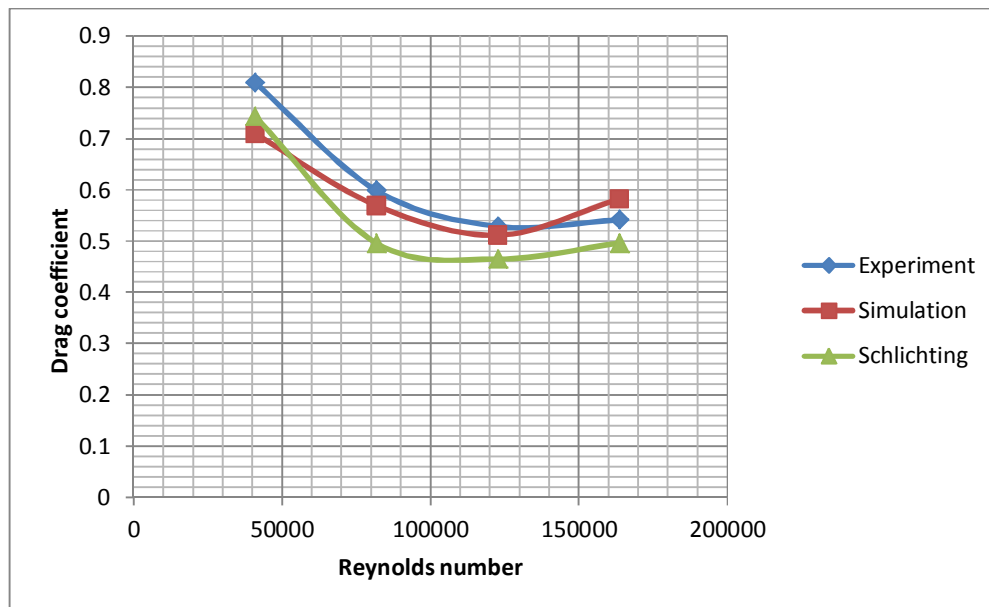


Figure 5.7 Drag coefficient versus Reynolds number (65mm)

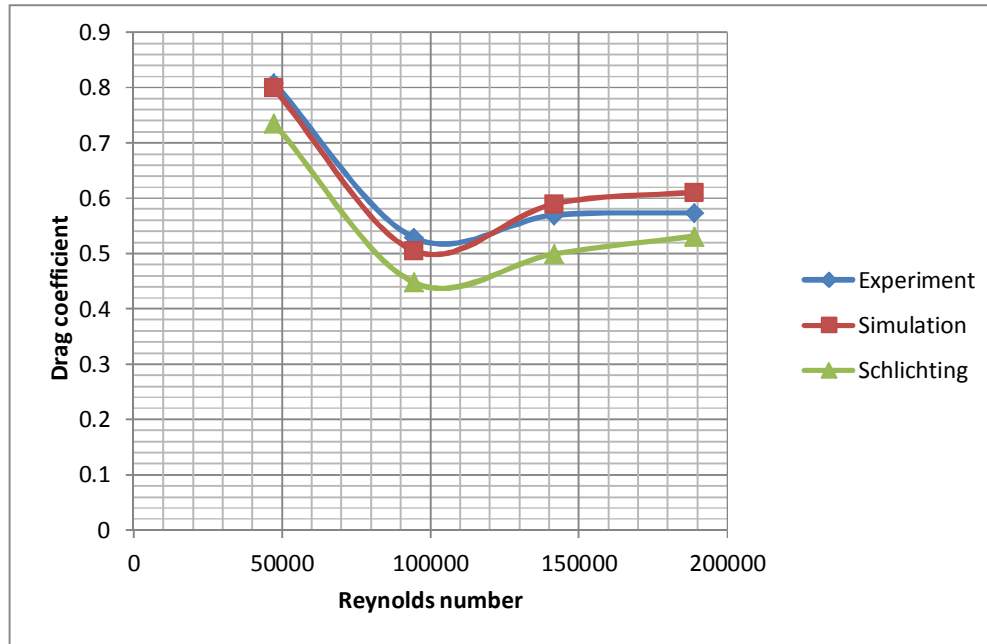


Figure 5.8 Drag coefficient versus Reynolds number (75mm)

5.4 Grid independence analysis

To make sure that results are independent of number of elements grid convergence must be done. Figure 5.9 presents drag force versus number of elements. It can be seen that when number of elements are reaching 350000, drag force becoming independent of number of elements.

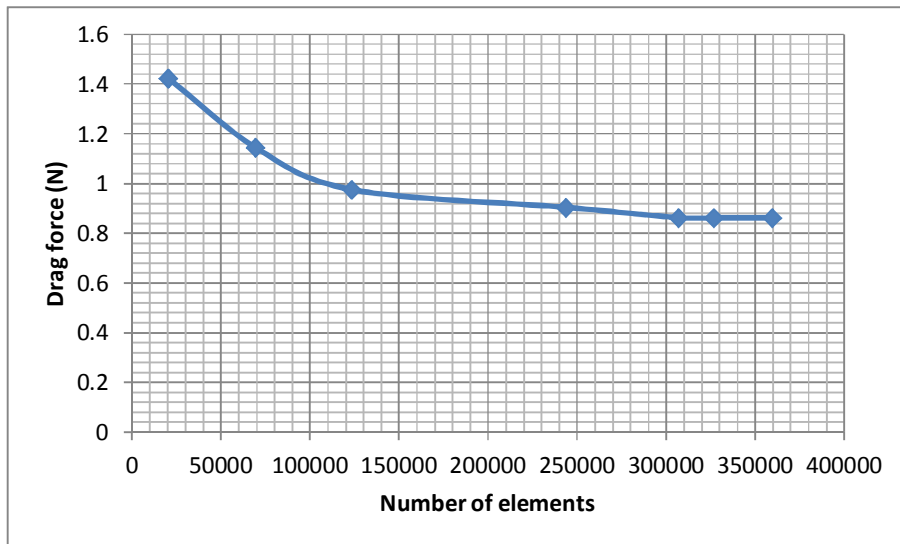


Figure 5.9 Drag force versus number of elements at 10m/s (32mm)

5.5 Mesh statistics results

Figure 5.10 presents mesh statistics from one of the simulation, which has the maximum values of skewness. As was discussed in Chapter 2, parameters such as skewness must be lower certain values. For tetrahedral mesh structure it must be lower than 0.9. In this simulation it is lower than 0.9, and is acceptable.

Statistics	
Nodes	130589
Elements	359684
Mesh Metric	Skewness
Min	3.56487297606622E-04
Max	0.863726755974925
Average	0.327729789213564
Standard Deviation	0.129104106937712

Figure 5.10 Mesh statistics from simulation

5.6 Discussion

As can be seen from Figure 5.1 and Figure 5.3, drag force is increasing with increasing wind speed and maintaining diameter constant, and vice versa. When speed is increasing it's obviously because pressure increases on the surface of cylinder, which increases drag force. Increasing in diameter will increase projected area exposed to flow, which also increases drag force. Figure 5.2, presents drag coefficient plot versus wind speed. This figure shows that increasing size will shift the graph to the right. However, they have intersection points. That means that drag coefficient is very sensitive to Reynolds number. After some wind speed for all sizes drag coefficient tends to become constant. As can be seen from Table 2.1, in supercritical regime drag coefficient is constant, also in critical regime it varies. In this experimental test, at highest speed and correlate drag coefficient flow regime is very close to supercritical. This is the reason why drag coefficient tends to become constant. From Figure 5.4 we see plot drag coefficient versus diameter. At low speeds, drag coefficient is higher compare to higher speeds. Increasing the speed, will decrease drag coefficient. However at 30 m/s and 40 m/s drag coefficient is about the same. For 32 mm diameter, there is a difference yet. However when it comes to bigger sizes, drag coefficient is same for these two speeds. Again this is because increasing the speed will increase Reynolds number, and it will come to constant critical regime, where drag coefficient has constant value. So after certain speed drag coefficient is independent of size, from Figure 5.2, constant speed for size2 and size4 is 30m/s. However for size1 and size3 this speed is 40 m/s. After 40m/s drag becoming totally independent of size.

CHAPTER 6

CONCLUSION

In this experiment, the drag coefficient of a circular cylinder was analyzed by conducting wind tunnel test and running simulation. Four different sizes of cylinder were tested at four various wind speeds. The sizes are 32, 50, 65 and 75 mm in diameter, the testing speeds are 10, 20, 30 and 40 m/s. The results were analyzed, plotted and compared with established data.

Increasing diameter of the cylinder, or wind speed while remaining one of them constant, will increase the drag force acting on the cylinder. Drag coefficient is very sensitive to Reynolds number. After certain speed drag coefficient becomes independent of size. On the plot drag coefficient versus wind speed, it can be seen that near supercritical region drag almost remains constant. At these values of Reynolds number, changing diameter won't affect the drag coefficient.

For size 1(32mm) and size 3(65mm) speed where drag coefficient becomes constant is 40 m/s, however for size 2(50mm) and size 4(75mm) this speed is 30 m/s. That means subcritical speed is dependent on cylinder size.

For all cylinder size, drag coefficient is independent after 40 m/s speed.

I would like to recommend for future research on the work performed on this thesis to vary the length of cylinder while keeping the diameter constant. The effects of size also can be studied by increasing number of cylinders.

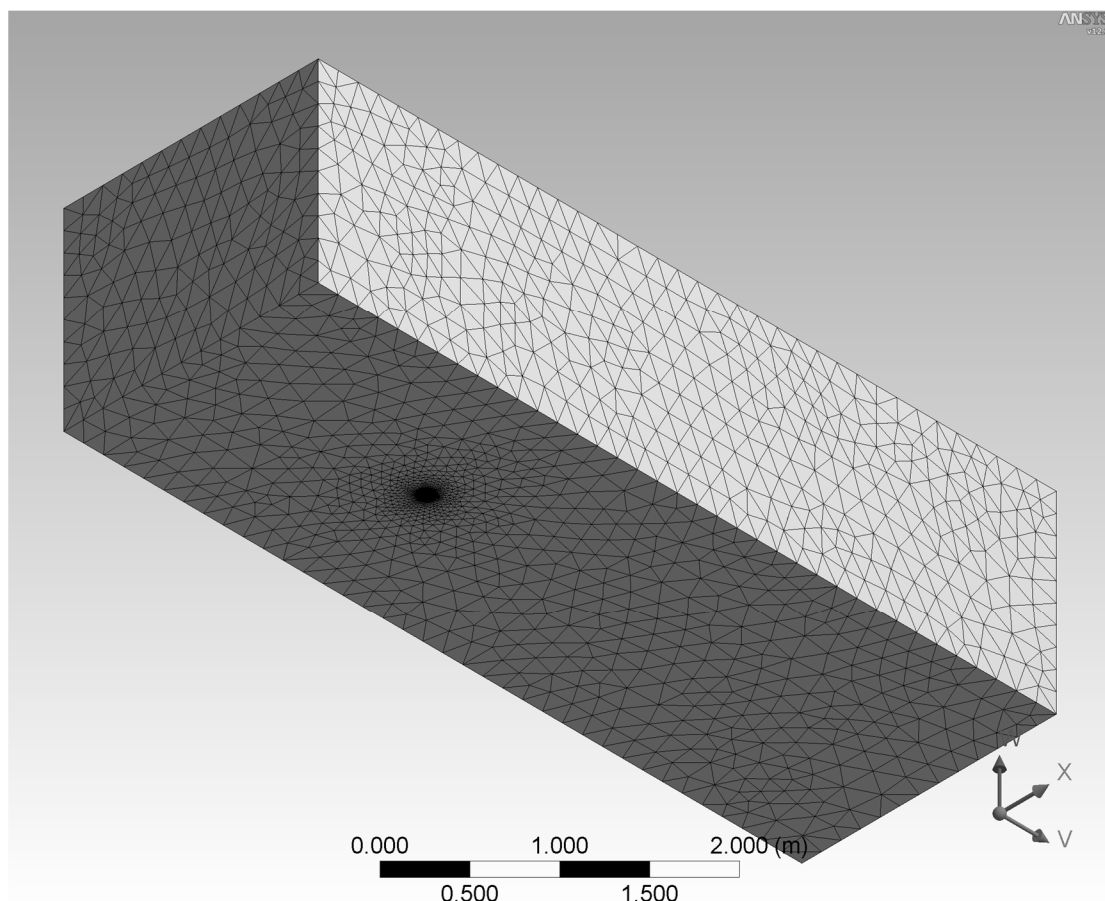
REFERENCES

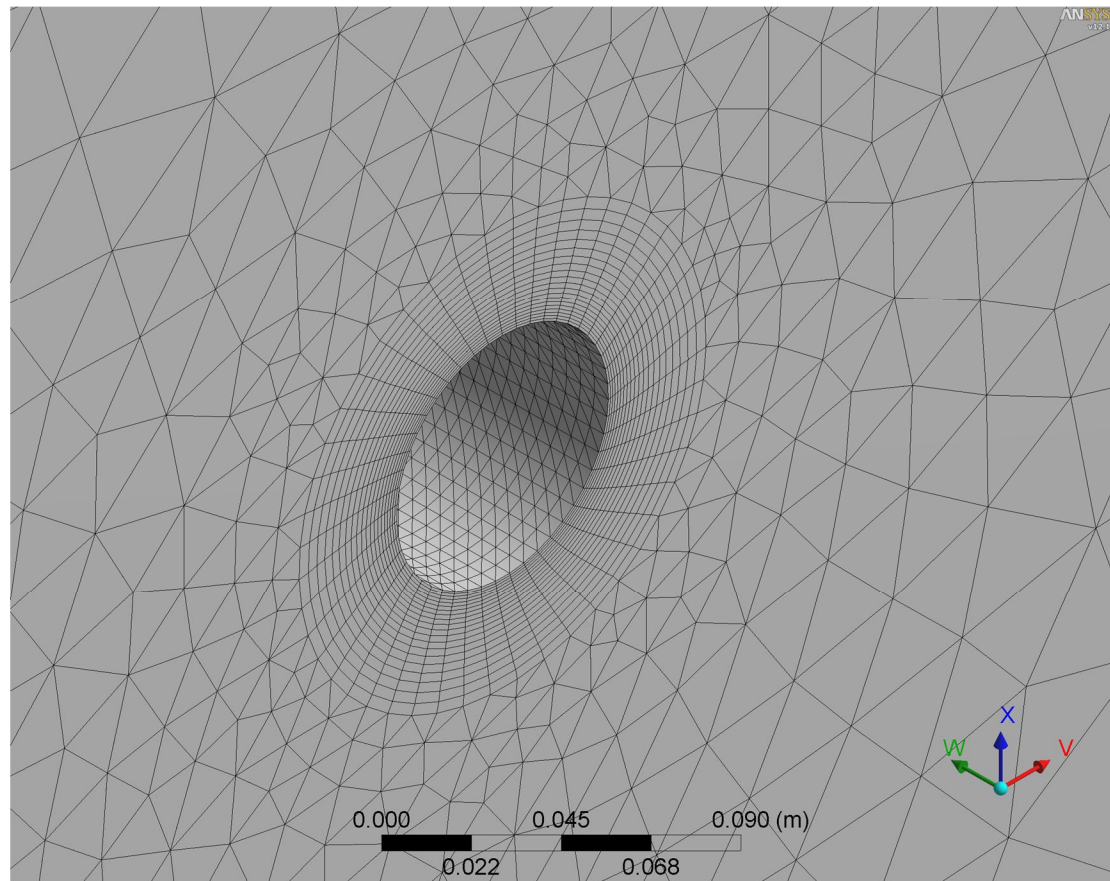
1. Anderson, John D. Jr. (2000). *Introduction to Flight*. (4th ed.) McGraw Hill Higher Education, Boston, Massachusetts, USA
2. Anderson, John D. Jr. (2007). *Fundamentals of Aerodynamics*. (4th ed.) McGraw-Hill Higher Education, Boston, Massachusetts, USA
3. Barlow, J.B. Rae, W.H. Jr, Pope A. (1999). *Low-speed wind tunnel testing*. (3rd ed.) John Wiley & Son, Inc.
4. Ching Jen Chen, Shenq-Yuh Jaw (1998). *Fundamentals of turbulence modeling*. Taylor & Francis
5. Finn, R. K. (1953). *Determination of the Drag on a Cylinder at Low Reynolds Numbers*. Journal Applied Physics. v24, pp.771-773.
6. Guven, O. Farell, C. and Patel, V.C. (1980). *Surface-roughness effects on the mean flow past circular cylinders*. Journal of Fluid Mechanics. v98, part 4, pp.673-701
7. Herriot, J.G. (1950). *Blockage Corrections for Three Dimensional-Flow Closed-Throat Wind Tunnels with Consideration of the Effect of Compressibility*. US: National Advisory Committee for Aeronautics.
8. Huner, B. and Hussey, R. G. (1977). *Cylinder Drag at Low Reynolds Number*. Phys. Fluids. v20, pp.1211-1218.
9. Katz, J. and Plotkin, A.(1991). *Low-speed aerodynamics*. McGraw-Hill
10. Merle, C. P. and Wiggert, D. C. (2007). *Schaum's Outline of Fluid Mechanics*. (2nd ed.) McGraw-Hill Professional
11. Roshko, A. (1961). *Experiments on the Flow Past a Circular Cylinder at Very High Reynolds Number*. Journal of Fluid Mechanics. v10, pp.345-356
12. Schlichting, H. (1979). *Boundary-Layer Theory*, New York: McGraw-Hill

13. Stangroom, P. *Computational fluid dynamics for wind farm optimization*, First year report for the degree of PhD, School of Civil Engineering. University of Nottingham; 2001
14. Tritton, D. J. (1988). *Physical Fluid Dynamics*. (2nd ed.) Oxford, England: Oxford University Press.
15. Versteeg, H. K. and Malalasekera, W. (1995). *An Introduction to Computational Fluid Dynamics*. England: Longman Group Limited, Longman House.
16. Zdravkovich, M.M. (1997). *Flow Around Circular Cylinders*. Vol. 1 Fundamentals. Oxford University Press
17. <https://confluence.cornell.edu/display/SIMULATION/FLUENT+Learning+Modules#FLUENTLearningModules-WhatisFLUENT>
18. http://www.engineeringtoolbox.com/air-absolute-kinematic-viscosity-d_601.html
19. <http://scienceworld.wolfram.com/physics/CylinderDrag.html>
20. <https://confluence.cornell.edu/display/SIMULATION/Home>
21. <http://www.vti.mod.gov.rs/vti/lab/tunel/ea-xbal.pdf>
22. <http://www.vti.mod.gov.rs/vti/lab/tunel/e-tunel-v.htm>
23. <http://www.allstar.fiu.edu/aero/Flow1.htm>
24. <http://www.fkm.utm.my/aerolab>
25. <http://en.wikipedia.org/wiki/Skewness>
26. <http://www.fluentusers.com>

APPENDIX A

Meshing of the domain



APPENDIX B**Inflation**

APPENDIX C

Sectioning of meshed cylinder

